Ultra-scalable Microring-based Architecture for Spatial-and-Wavelength Selective Switching

Liang Yuan Dai[1], Vignesh Gopal[1] and Keren Bergman[1]
1. Department of Electrical Engineering, Columbia University, 500 W 120th St., New York, New York, USA
ld2719@columbia.edu

***Abstract*—We introduce a novel microring-based architecture for spatial-and-wavelength selective switching, reducing the switch elements required for non-blocking operations by an order of magnitude. The fabricated 4×4×4λ silicon photonics network demonstrates more than 40 dB of crosstalk suppression, and negative to zero power penalties per path.**

***Index Terms*—silicon photonics, optical switch, optical network, microring resonator**

I. Introduction

Optical interconnects have solidified themselves as vital components in today's datacenter networks [1]. The main functionality of an integrated optical switch fabric can generally be classified into two categories: broadband (or simply spatial) switching and narrowband (or wavelength-selective) switching. To introduce wavelength-level switching granularity to spatial switches, as desired by disaggregated high-performance computing architectures with wavelength-division multiplexed (WDM) signals [2], we have seen past demonstrations [3], [4] parallely combine spatial switching planes with wavelength (de)multiplexers. A condensed spatial-and-wavelength selective switch (SWSS) topology has also been implemented in [5], utilizing microring resonators MRRs as both spatial and wavelength filters. The cost of integrating these two domains, however, is an exponential increase in the total number of switch elements (SE), which is especially noticeable at scale (Fig.1b). The authors of [5] attempted to address this issue via a revised hybrid broadband crossbar topology in [6], halving the number of SEs. To date, the best scaling SWSS topology would be a three-stage Clos, using an MZI-based wavelength selective switch as its fundamental SE, presented in [7]. In this work, we present the best scaling non-blocking SWSS architecture by nearly an order of magnitude. We have fabricated a $4 \times 4 \times 4\lambda$ illustrating our topology, which demonstrated on-chip loss of 1.54 dB, crosstalk suppression of more than 40 dB, and zero to negative power penalties for the paths evaluated.

II. Spatial-and-Wavelength Selective Switching Architecture

The generalized design of our novel switching architecture can be seen in Fig.1a, in a double-crosspoint arrangement. The top half of the double-crosspoint serves as wavelength-selective demultiplexers, where individual WDM channels are

This work was supported by the U.S. Advanced Research Projects Agency–Energy under ENLITENED Grant DE-AR000843. The chip fabrication and custom device processing were provided by AIM Photonics/SUNY Poly Photonics engineering team and fabricator in Albany, New York.

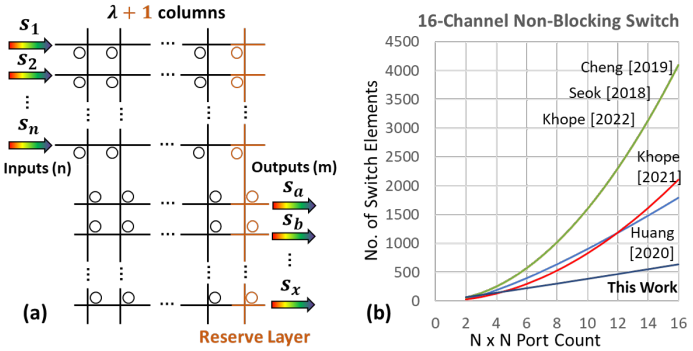

Fig. 1. a) The generalized double-crosspoint for the proposed spatial-and-wavelength selective switch design. b) The scaling comparisons with other state-of-the-art SWSS, from $2 \times 2 \times 16\lambda$ to $16 \times 16 \times 16\lambda$. Higher-order resonators which only handle a single wavelength is counted as one SE

dropped onto the column buses by microring resonators. The channels on the column buses are then serviced by the bottom half of the switch, which behave as wavelength-selective multiplexers. By combining the multiplexing and demultiplexing aspects of the double-crosspoint topology, this switch fabric allows for individual manipulation of wavelength channels to deconstruct, interlace, and reconstruct WDM signals - thus WDM inputs S_1, S_2, and S_n can be used to create new outputs of S_a, S_b, and S_x. To attain rearrangable non-blocking (RNB) switching capabilities, an additional column bus of resonators are required (the reserve layer) to route possibly conflicting wavelength channels in a subset of switching scenarios.

Fig.2 illustrates two routing schemes for a $2 \times 2 \times 4\lambda$ double-crosspoint switch. Here, each WDM channel traversing the switch can be characterized by their input, output, and wavelength, and is designated by the following notation:

$$S^{\lambda}_{input,output} \tag{1}$$

In Fig.2a, the wavelength channels of the WDM inputs are demultiplexed, interlaced, then recombined to form two new WDM signals at distinct spatial outputs. Colored rings indicate the tuning of the microring resonances to the specific

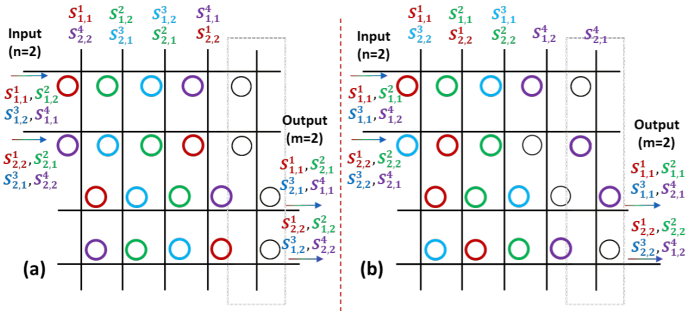

Fig. 2. a) Example routing of two 4λ WDM signals, with interlaced channels in a $2 \times 2 \times 4\lambda$ double-crosspoint SWSS. b) Example of routing scenario requiring usage of the reserve layer

2023 IEEE Silicon Photonics Conference (SiPhotonics) | 978-1-6654-8655-2/23/$31.00 ©2023 IEEE | DOI: 10.1109/SIPHOTONICS55903.2023.10141951

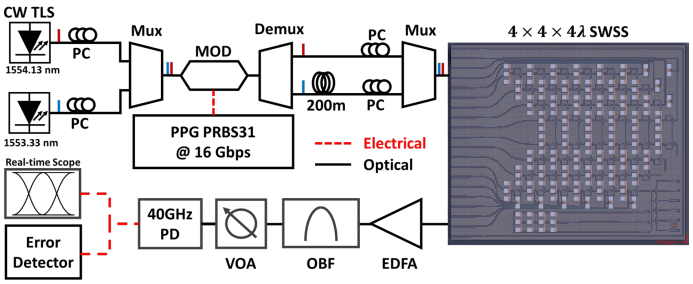

Fig. 3. Full experimental setup, with micrograph of the fabricated SWSS. CW TLS - Continuous Wave Tunable Laser Source. PC - Polarization Controller. Mux - optical multiplexer. Demux - optical demultiplexer. EDFA - Erbium-Doped Fiber Amplifier. OBF - Optical Bandpass Filter. VOA - Variable Optical Attenuator. PD - Photodetector.

channels in questions. Here, we see that each vertical bus can be occupied by more than one channel (indicated by the signals above the columns). In fact, if signals are distinct in their input, output, and wavelength, then they are able to share the same vertical bus. By exploiting this property, the double-crosspoint topology is able to achieve its major reduction in the number of SE required for a given radix.

With that said, the uniqueness condition imposed by the columns also creates opportunities for conflict, as illustrated in Fig.2b. Here, we arrive at a situation of where it is necessary to use a reserve layer in order to achieve full routing, as it is not possible to cascade $S^4_{1,2}$ and $S^4_{2,1}$ on the same bus. In fact, there is no method of non-blocking routing for this set of signals without the reserve layer, regardless of the tuning permutation for the microring resonances. However, it can be proven with the use of vertex-coloring and Hall's Theorem that only one reserve layer is required to maintain RNB, for any $n \times m \times \lambda$ double-crosspoint SWSS, given $n <= m <= \lambda$. The total number of SE required for an $n \times m \times \lambda$ switch is thus:

$$SE = (n + m)(\lambda + 1) \tag{2}$$

III. Experimental Testing and Link-Level Demonstration

A $4 \times 4 \times 4\lambda$ SWSS network has been fabricated through AIM Photonic, using foundry specific PDK elements. The photonic integrated circuit (Fig.3) measures $2.5mm \times 3.0mm$, and is experimentally characterized at the die-level. The implemented switch elements are second-order resonators, created by via cascading the drop port of one microring filter with the input of another, in an effort to increase crosstalk suppression. They demonstrate an off-resonance insertion loss of 0.2 dB, and a through loss of 0.7 dB. Their extinction ratio have been measured to be greater than 40 dB, limited by the resolution of the optical spectrum analyzer (Fig.4 inset).

The full link-level experimental setup can be seen in Fig.3, where two decorrelated 16 Gb/s optical NRZ signals, spaced 100 GHz apart, are sent through the switch fabric. The output is amplified by an EDFA to compensate for coupling loss, before entering an optical bandpass filter (OBF) to focus on the channel of interest. A variable optical attenuator (VOA) combined with a 33 GHz photodetector (PD) and an Error Detector are used to generate the BER curves seen in Fig.4.

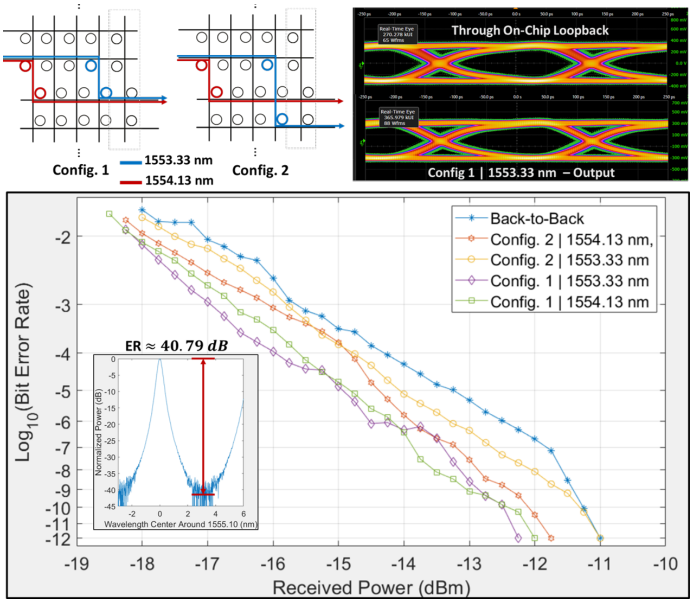

Fig. 4. Bit error rate curves for the two switching configurations demonstrated, with eye diagrams comparing the back-to-back link and a link through the switch. Inset: Spectrum response of a single second-order SE.

Two switching configurations were demonstrated as part of our link performance analysis. Configuration 1 mimics broadband switching, whereas configuration 2 mimics wavelength-selective switching. In all cases, we see a zero to negative power penalty imposed on the link, which can be attributed to the filtering effects of the microring paths [8].

IV. Conclusion

We have demonstrated a novel spatial-and-wavelength selective switching architecture, capable of rearrangeably non-blocking routing and requires a magnitude fewer switch elements to instantiate. The fabricated $4 \times 4 \times 4\lambda$ SWSS fabric has shown high crosstalk suppression of greater than 40 dB, and a negative power penalty impact on the routed links, which indicate further scaling gains are achievable with our proposed topology.

References

[1] L. Poutievski *et al.*, "Jupiter evolving: transforming google's datacenter network via optical circuit switches and software-defined networking," in *Proceedings of the ACM SIGCOMM 2022 Conference*, 2022, pp. 66–85.

[2] H. Ballani *et al.*, "Sirius: A flat datacenter network with nanosecond optical switching," in *Proceedings of the Annual conference of the ACM Special Interest Group on Data Communication*, 2020, pp. 782–797.

[3] T. J. Seok *et al.*, "Mems-actuated 8× 8 silicon photonic wavelength-selective switches with 8 wavelength channels," in *CLEO: Science and Innovations*. Optica Publishing Group, 2018, pp. STu4B–1.

[4] Q. Cheng, M. Bahadori, M. Glick, and K. Bergman, "Scalable space-and-wavelength selective switch architecture using microring resonators," in *CLEO*. IEEE, 2019, pp. 1–2.

[5] A. S. P. Khope *et al.*, "Compact wavelength selective crossbar switch with cascaded first order micro-ring resonators," in *Photonics*, vol. 9, no. 2. MDPI, 2022, p. 60.

[6] A. S. Khope *et al.*, "Scalable multicast hybrid broadband-crossbar wavelength selective switch: proposal and analysis," *Optics Letters*, vol. 46, no. 2, pp. 448–451, 2021.

[7] Y. Huang, Q. Cheng, A. Rizzo, and K. Bergman, "High-performance microring-assisted space-and-wavelength selective switch," in *Optical Fiber Communication Conference*, 2020, pp. Th2A–7.

[8] Y.-H. Hung *et al.*, "Silicon photonic switch-based optical equalization for mitigating pulsewidth distortion," *Optics Express*, vol. 27, no. 14, pp. 19 426–19 435, 2019.